June 2005

Electronic Properties of Silicon Nanowires

Yun Zheng

Christian Rivas

Roger Lake

Khairul Alam

Timothy B. Boykin
University of Alabama, Huntsville

See next page for additional authors

Electronic Properties of Silicon Nanowires

Yun Zheng, Cristian Rivas, Roger Lake, *Senior Member, IEEE*, Khairul Alam, *Member, IEEE*, Timothy B. Boykin, *Member, IEEE*, and Gerhard Klimeck, *Member, IEEE*

***Abstract*—The electronic structure and transmission coefficients of Si nanowires are calculated in a $sp^3d^5s^*$ model. The effect of wire thickness on the bandgap, conduction valley splitting, hole band splitting, effective masses, and transmission is demonstrated. Results from the $sp^3d^5s^*$ model are compared to those from a single-band effective mass model to assess the validity of the single-band effective mass model in narrow Si nanowires. The one-dimensional Brillouin zone of a Si nanowire is direct gap. The conduction band minimum can split into a quartet of energies although often two of the energies are degenerate. Conduction band valley splitting reduces the averaged mobility mass along the axis of the wire, but quantum confinement increases the transverse mass of the conduction band edge. Quantum confinement results in a large increase in the hole masses of the two highest valence bands. A single-band model performs reasonably well at calculating the effective band edges for wires as small as 1.54-nm square. A wire-substrate interface can be viewed as a heterojunction with band offsets resulting in reflection in the transmission.**

***Index Terms*—Nanowires (NWs), silicon nanowires (SiNWs).**

I. Introduction

SEMICONDUCTOR nanowires (NWs) have been widely studied as nanoscale building blocks for nanoelectronics, since they can function both as devices and wires that access the devices. NWs are synthesized from a range of different materials [1], such as CdS and ZnS [2], GaN [3], p-GaN [4], Si, Ge [5], [6], or InP [7], [8]. They have been assembled as field-effect transistors (FETs) [8], [9], inverters [10], photodetectors [11], nanosensors [12], [13], light-emitting diodes and lasers [8], [14], decoder [15], nonvolatile memory and programmable logic [16]–[18].

Simulations have been done to study the structures, electronic spectra, and transport properties of Si nanowires (SiNWs) [19]–[21]. Thermal conductivity [22], [23] and optical properties [24] of SiNWs have also been studied. From an applications point of view, it has been shown that doped p type and n type SiNWS can be assembled to form p-n junctions, bipolar transistors, and complementary inverters [10], [25]. These results have lead to the suggestion that SiNWs may become crucial components for nanoscale electronics [9].

For this reason, we find it timely to study the electronic properties of SiNWs such as the band gap, valley splittings, and effective masses as functions of wire dimension. The band gap, valley splittings, and effective masses are all relevant to the performance of ultrascaled FETs built with SiNWs. An increased bandgap exponentially suppresses parasitic interband tunneling which is a limit to scaling of Si FETs [26]. For a wire grown in a $\langle 100 \rangle$ direction, valley splitting in the conduction band pushes up the two electron Δ valleys aligned along the axis of the wire which reduces the effective mobility mass in the transport direction. Quantum confinement pushes up the conduction band minimum composed of the four Δ valleys whose long axis is perpendicular to the wire axis. This results in a transverse mass increased by about 35% for 2.5-nm-thick wires. The corresponding hole masses are increased by a factor of about six. The effective mass affects both the mobility and the density of states. Even for ultrascaled FETs, there are indications that mobility will still be a relevant parameter governing performance metrics [27]. The density of states directly enters into the quantum capacitance and current drive which also affects the performance of ultrascaled FETs [28].

The small splitting of the 4 valleys forming the conduction band minimum is relevant to quantum computing implementations based on Kane's original proposal [29]. Lifting the conduction bandedge degeneracy would remove the fast oscillating factors in the exchange coupling between donors making donor placement much less critical [30], [31].

For rapid design calculations, it would be convenient to be able to use a simple model such as a single-band effective mass model for calculating the properties of SiNWs. Therefore, we assess the validity of the single-band model by comparing the results calculated from that model to those obtained from a full-band model.

II. Approach

We consider two types of structures, ideal infinite Si wires passivated with H, and semi-infinite Si wires sitting on a planar Si substrate also passivated with H. Fig. 1 on the left shows the

Manuscript received July 1, 2004; revised March 4, 2005. This work was supported in part by the National Science Foundation (NSF) under Grant DMR-0103248, the Department of Defense (DoD), Defense Advanced Research Projects Agency (DARPA), and the Defense Microelectronics Activity (DMEA) under Grant DMEA90-02-2-0216, and in part by the Microelectronics Advanced Research Corporation Focus Center on Nano Materials (FENA). This work was performed in part at the Jet Propulsion Laboratory, California Institute of Technology, under a Contract with the National Aeronautics and Space Administration. Support for G. Klimeck was provided by the Advanced Research and Development Activity (ARDA), the Office of Naval Research (ONR), and the NSF under Grant EEC-0228390. Computer simulations were performed on the University of California, Riverside (UCR) Institute of Geophysics and Planetary Physics (IGPP) Beowulf computer Lupin. The review of this paper was arranged by Editor S. Datta.

Y. Zheng, R. Lake, and K. Alam are with the Department of Electrical Engineering, University of California, Riverside, CA 92521-0204 (e-mail: rlake@ee.ucr.edu) USA.

C. Rivas is with the Eric Jonson School of Engineering, University of Texas at Dallas, Richardson, TX 75083 USA.

T. Boykin is with the University of Alabama, Huntsville, Huntsville, AL 35899 USA.

G. Klimeck is with the Department of Electrical and Computer Engineering, Purdue University, W. Lafayette, IN 47907-1285 USA, and also with the Jet Propulsion Laboratory, California Institute of Technology, Pasadena, CA 91109 USA.

Digital Object Identifier 10.1109/TED.2005.848077

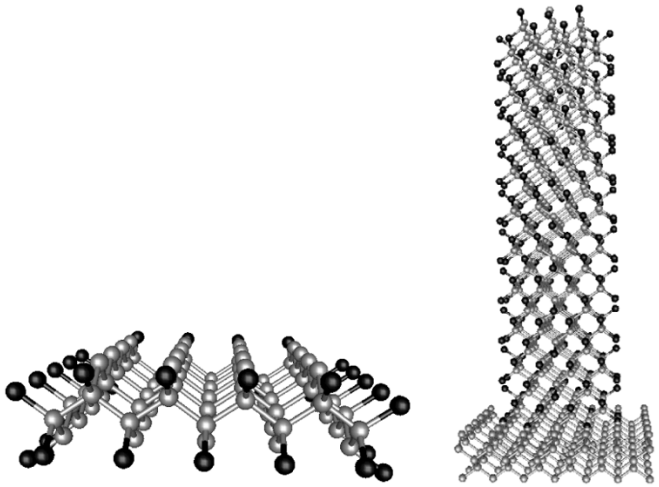

Fig. 1. (Left) unit cell of the 1.54-nm square Si wire passivated with H. (right) H passivated octagonal Si wire on a substrate. The distance between opposite faces is 1.15 nm.

unit cell of an ideal 1.54-nm square Si wire passivated with H. Fig. 1 on the right shows elevations of a Si wire on a Si substrate. The grey atoms are Si and the black ones are H. The ideal wires are square with sides along equivalent $\langle 110 \rangle$ directions and their long axis along the $[001]$ direction. The wire on substrate is round or, more exactly, octagonal with faces along the equivalent $\langle 110 \rangle$ and $\langle 100 \rangle$ directions.

Two different models are used. The first is a three-dimensional (3-D) discretization of the single-band effective mass equation. This model is of interest for fast design calculations, so we assess its accuracy and utility by comparing its results with those from the fullband model.

The single-band effective mass equation is solved by finite difference on a square grid aligned along the x, y and z directions with a grid spacing Δ of approximately 2 Å chosen to give a good fit to the square box in x and y. Hamiltonian matrix elements to points on the grid that lie outside of the box are set to 0, the equivalent of hard wall boundary conditions. The effective mass equation is discretized to include the longitudinal and transverse effective masses of Si. For example, the diagonal element resulting from the kinetic energy term is $(\hbar^2/\Delta^2)[(1/m_x) + (1/m_y) + (1/m_z)]$. The nearest neighbor off-diagonal elements are $t_i = \left(-\hbar^2/2m_i\Delta^2\right)$ where $i = x$, y, or z, and t_i is the matrix element coupling nearest-neighbor grid points in the x, y, or z directions. To simulate the Δ valley near (100) for electrons, $m_x = m_l$, $m_y = m_t$, and $m_z = m_t$ where $m_l = 0.98\ m_0$ and $m_t = 0.19\ m_0$ are the longitudinal and transverse electron masses of Si, respectively. For the valence band, the averaged density of states masses are used for all directions: $m_{\mathrm{HH}} = 0.49\, m_0$, $m_{\mathrm{LH}} = 0.16\, m_0$, and $m_{\mathrm{SO}} = 0.24\, m_0$.

The open boundaries on the ends are included via boundary self-energies calculated from the surface Green functions of the semi-infinite regions above and below the NW. The wire consists of layers of grid points in the z direction. Layers $\{-\infty, \ldots, 0\}$ lie in the left contact. Layers $\{1, \ldots, N\}$ lie in the "device" and layers $\{(N+1), \ldots, \infty\}$ lie in the right contact. The surface Green functions are calculated using [32, Eqs. (A1) and (A2)] similar to those described first in [33]. The surface Green functions are, for the semi-infinite region below the NW

$$g_s = \left[(E + i\eta)\mathbf{I} - \mathbf{D}_{0,0} - \mathbf{t}_{0,-1}\boldsymbol{\chi}_L \mathbf{z}_L^{-1} \boldsymbol{\chi}_L^{-1}\right]^{-1} \quad (1)$$

and for the semi-infinite region above the NW

$$g_s = \left[(E + i\eta)\mathbf{I} - \mathbf{D}_{n+1,n+1} - \mathbf{t}_{n+1,n+2}\boldsymbol{\chi}_R \mathbf{z}_R \boldsymbol{\chi}_R^{-1}\right]^{-1} \quad (2)$$

where we have used block matrix notation. Each bold symbol represents an $M \times M$ matrix where M is the number of grid points in a layer. E is the energy and $i\eta$ is an imaginary potential that is nonzero only in the leads. For these calculations, $\eta = 5$ meV. The $\mathbf{D}s$ are the intra-layer blocks of the Hamiltonian and the $\mathbf{t}s$ are the inter-layer blocks of the Hamiltonian. The numerical subscripts and n refer to layer indexes in the z direction.

The procedure is exactly as described following [32, Eqs. (A1) and (A2)]. The matrix of generalized eigenvectors $\boldsymbol{\chi}$ and eigenvalues $\mathbf{z}$ are calculated from the generalized eigenvalue equation described in [34]. They are sorted into left and right moving eigenstates as described in the text surrounding [32, Eq. (A14)] where $t_{c,a}$ is, in the single-band model, $\mathbf{t}_{n,n+1}$. The subscripts L and R indicate whether the matrices are composed of the left or right moving states, respectively. In this case, left moving indicates propagation in the negative z direction and right moving indicates propagation in the positive z direction.

The second model is the nearest neighbor $sp^3d^5s^*$ model, where the Hamiltonian matrix elements, (described by Boykin *et al.*, [35]) are optimized with a genetic algorithm. Previous calculations by others [21] and ourselves [36] used the $sp^3d^5s^*$ parameters of [37]. Table I shows a comparison of bulk Si properties calculated from those parameters and the ones optimized by Boykin *et al.* [35] that we use here. Since we focus on the effect of confinement on the effective mass, we felt that it was important to begin with bulk values that were as accurate as possible. The bulk values of the longitudinal and transverse electron masses obtained from the parameters of [35] are significantly closer to the experimentally accepted values than those of [37].

In the $sp^3d^5s^*$ model, the surface of the Si NW in x and y is treated in a similar way to that of the discretized single-band model described above. Matrix elements to Si atoms that fall outside of the device domain are set to zero. The Si atoms that are the nearest neighbors to the ones within the device domain are replaced with H atoms to get rid of the surface states. Our perspective on the H atoms is that they are simply a numerical method to eliminate the surface states. The perspective is identical to that described by Lee *et al.* [38] in which they state that, "The proper BC for a reduced buffer should efficiently eliminate all nonphysical surface states and at the same time should minimally affect physical interior states." Lee *et al.* transformed the atomic orbital basis into the hybridized sp^3 orbitals, increased the energy of the surface dangling ones well above the energy range of interest, and then transformed back into the atomic orbital basis. We used a genetic algorithm to determine H parameters to produce the same effect of eliminating the surface states. On each H atom, there is one s orbital. Its nonzero matrix elements with the Si atomic orbitals consist of V_{ss}, $V_{sp\sigma}$, V_{ss^*},

TABLE I
K MINIMA (AS A PERCENT OF THE $X-\Gamma$ DISTANCE) AND EFFECTIVE MASSES (IN UNITS OF THE FREE-ELECTRON MASS)

Quantity	$k_{min}^{[100]}$	$m_{X,l}^{[100]}$	$m_{X,t}^{[100]}$	$m_{hh}^{[100]}$	$m_{lh}^{[100]}$	$m_{so}^{[100]}$
Jancu Phys. Rev. B **57**, 6493 (1998)	84.5%	0.706	0.230	0.245	0.212	0.233
Boykin Phys. Rev. B **69**, 115201 (2004)	81.3%	0.891	0.201	0.276	0.214	0.246

TABLE II
HAMILTONIAN MATRIX ELEMENTS FOR HYDROGEN IN eV

ϵ_s	V_{ss}	V_{ss^*}	$V_{sp\sigma}$	$V_{sd\sigma}$
0.9998400	-3.999720	-1.697700	4.251750	-2.105520

and $V_{sd\sigma}$ as shown in Table II. Surface reconstruction is not considered.

The transmission coefficients are calculated using the nonequilibrium Green function (NEGF) formalism with a recursive Green function algorithm. The algorithms are described in detail in [39]. Transmission coefficients that we plot are summed over all spin and orbital channels at a given energy. Formally, they are defined by $T(E) = \mathrm{tr}\{G^R\Gamma^L G^A \Gamma^R\}$ where the trace is over all orbitals and the notation corresponds to that of [39].

We calculate the $E-k$ dispersion relation of the wires, and we calculate transmission coefficients for wires of 16 unit cells. For the $E-k$ calculations and valence band transmission calculations, spin-orbit coupling is included. For the conduction band transmission coefficients, spin-orbit coupling is ignored since we found that it had no noticeable effect on the results. We calculate transmission coefficients for a wire on a substrate as shown in Fig. 1 and compare to an ideal wire. We also compare transmission coefficients for a 1.54-nm wire, calculated from both the fullband and single-band models.

III. NUMERICAL RESULTS

Fig. 2 shows a typical energy versus wavevector relation for a Si NW. In this case, the NW is 1.54-nm square. The conduction band edge at Γ in the one dimensional (1-D) Brillouin zone is formed from the four equivalent Δ valleys of the bulk Si, and it is therefore labeled Δ_4 in the figure. The next higher valleys are formed from the two equivalent Δ valleys (Δ_2) which point along the vertical $[001]$ axis of the Si wire. The 1-D Brillouin zone of the Si wire is 1/2 as long as the length of the bulk Si Brillouin zone along the Δ line. In real space, the 1-D Si $[001]$ wire primitive unit cell consists of four atomic layers, whereas the bulk 3-D Si primitive unit cell consists of two Si atoms. The position in the 1-D Brillouin zone of the Δ_2 valley minimums at 0.37 π/a can be qualitatively understood in terms of zone folding. The Δ_2 valley minimum which in bulk Si occurs at 0.81 $2\pi/a$ (with our parameters), is folded back into the first half of the 1-D Brillouin zone.

In the valence band, there is significant mixing and splitting of the hole bands. The bandgap is increased by quantum confinement. For reference, for bulk Si, the valence band edge is at

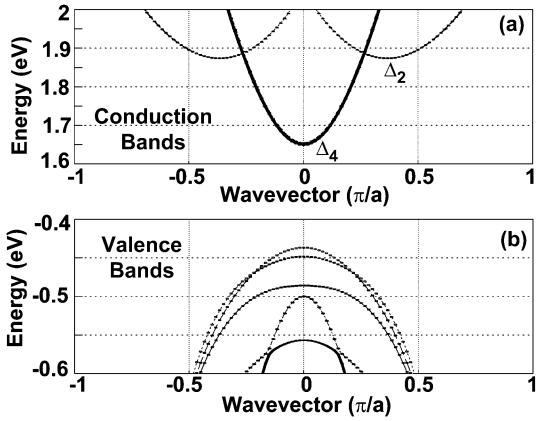

Fig. 2. Si 1.54 × 1.54-nm NW band structure calculated from the empirical tight-binding $sp^3d^5s^*$ model. (a) Conduction bands and (b) valence bands. The lattice constant $a = 5.4$ Å.

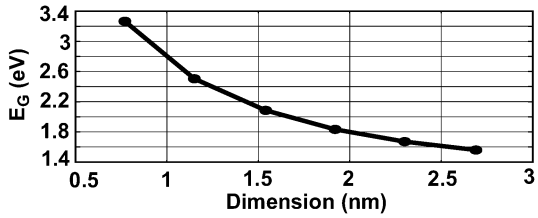

Fig. 3. Si NW bandgap versus Si wire thickness.

$E = 0$ and the conduction band edge is at $E = 1.13$ eV. In the 1-D Brillouin zone of a wire, Si is a direct gap material.

In Figs. 3–7, we display the results of calculations of band energies and effective masses for a series of ideal wires corresponding to unit cells as shown in Fig. 1 with dimensions ranging from 0.8×0.8 nm (5×5 atoms) to 2.7×2.7 nm (15×15 atoms).

Fig. 3 shows the effect of quantum confinement on the bandgap as a function of wire thickness. The bandgap is 2.5 eV for a 1.2-nm wire and it falls to 1.56 eV for a 2.7-nm wire.

Fig. 4 shows the effect of wire thickness on the (a) Δ_2 and Δ_4 conduction band valley energies, (b) the $\Delta_2 - \Delta_4$ splitting, and (c) the splitting at the conduction band minimum labeled Δ_4 in Fig. 2. The $\Delta_2 - \Delta_4$ splitting results from the different quantum confinement energies for the Δ_2 and Δ_4 valleys. In a single-band picture, the effective mass of the Δ_2 valleys in the direction of the confinement is the transverse electron mass. The effective mass of the Δ_4 valleys in the direction of the confinement is a combination of both the longitudinal and transverse electron masses. The splitting is 285 meV for the 1.2-nm wire and it falls to 117 meV for the 2.7-nm wire.

The splitting at the conduction band minimum shown in Fig. 4(c) is a two-dimensional analogue of the splitting recently investigated in planar Si quantum wells [40]. Lifting the degeneracy of the lowest conduction band state is useful for quantum computing implementations based on Kane's model [29]–[31]. In Fig. 4(c) the lowest energy is the reference energy $(E = 0)$ for each wire dimension. The conduction band minimum is composed of four valleys from the bulk Si. It thus can split into four values as opposed to the two values for the planar quantum wells analyzed in [40]. However, for wires greater

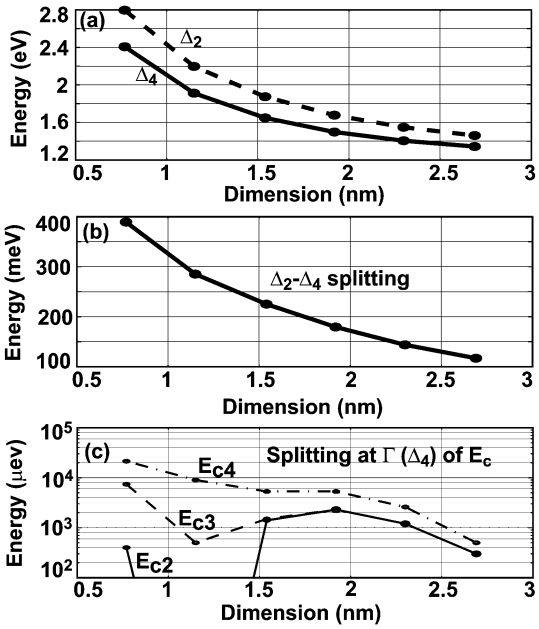

Fig. 4. Effect of Si wire thickness on the (a) Δ_2 and Δ_4 conduction band valleys, (b) the $\Delta_2 - \Delta_4$ splitting, and (c) the splitting at the conduction band minimum labeled Δ_4 in Fig. 2. In (c), the lowest conduction band energy for each wire cross section is used as the reference energy and set to 0. The next three highest band energies are labeled E_{c2}, E_{c3}, and E_{c4}, respectively. At 1.2 nm, E_{c2}, is closely degenerate with E_{c1} and thus off the scale of the plot.

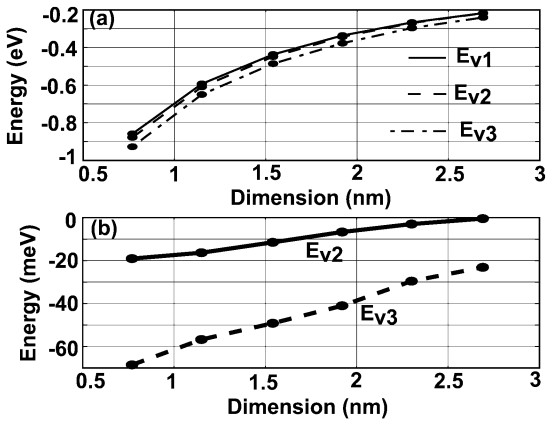

Fig. 5. Effect of Si wire thickness on (a) the maximum energy of the three highest valence bands and (b) their energy splitting. In (a), the three highest valence band energies are labeled from high to low, E_{v1}, E_{v2}, and E_{v3}, respectively. For each thickness in (b) the highest valence band energy [E_{v1} from (a)] is used as the reference at $E = 0$. The energies E_{v2} and E_{v3} are plotted with respect to E_{v1}.

than 1.54 nm, the two middle energies become essentially degenerate, and they are split evenly between the lowest and highest energy. For the 1.2-nm wire, the two lowest energies are degenerate. We also observe oscillatory and decay behavior as is seen in the planar quantum wells.

The Δ_2 conduction band valley is composed of the two ellipses which lie along the axis of the wire. The confinement does not couple these valleys, so splitting is neither expected nor observed in the Δ_2 valleys.

Fig. 5 shows the effect of quantum confinement on the three highest valence bands and their splitting as a function of wire thickness. In Fig. 5(b), the energy of the highest valence band is used as the reference energy corresponding to $E = 0$ for each wire dimension.

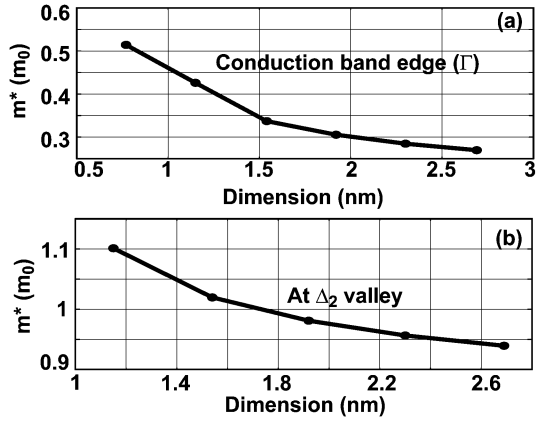

Fig. 6. Conduction electron effective masses versus wire thickness at (a) the conduction band minimum and (b) the Δ_2 valley.

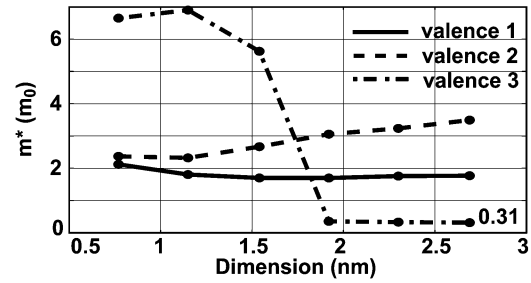

Fig. 7. Effective masses of the three highest valence bands as a function of wire thickness. In the legend, the valence bands are numbered from the highest energy to the lowest so that "valence 1" corresponds to the highest energy valence band, "valence 2" corresponds to the second highest energy valence band, and "valence 3" corresponds to the third highest energy valence band.

Fig. 6 shows the conduction electron effective masses versus wire thickness at (a) the conduction band minimum and at (b) the Δ_2 valley. These masses are calculated from the $E - k$ dispersion relations such as that shown in Fig. 2 from the relation $(1/m^*) = (1/\hbar^2)(\partial^2 E/\partial k^2)$. Since the conduction band minimum is composed of the four Δ valleys with the transverse mass in the direction of the axis of the wire, one would expect the effective mass of the conduction band minimum to correspond to the bulk Si electron transverse mass equal to $0.2\ m_0$ in this model. The value of $0.27\ m_0$ for the thickest wire (2.7 nm) is 35% greater than the bulk value. The Δ_2 valley is composed of the two ellipses which lie along the axis of the wire, and thus one would expect the effective mass to correspond to the longitudinal electron effective mass equal to $0.89\ m_0$ in this model. For the thickest wire, the mass is $0.94\ m_0$. The valley splitting reduces the averaged mobility mass along the axis of the wire, but quantum confinement increases the transverse mass of the conduction band edge.

The effect of confinement on the effective mass is most pronounced in the valence band. Fig. 7 shows the valence band effective masses for each wire thickness. For the wire thickness range (0.8–2.7 nm) that we have considered, the effective [100] mass for the highest valence band is at least six times heavier than that for the bulk heavy hole, and the second highest band is even heavier. The effective mass for the third highest band

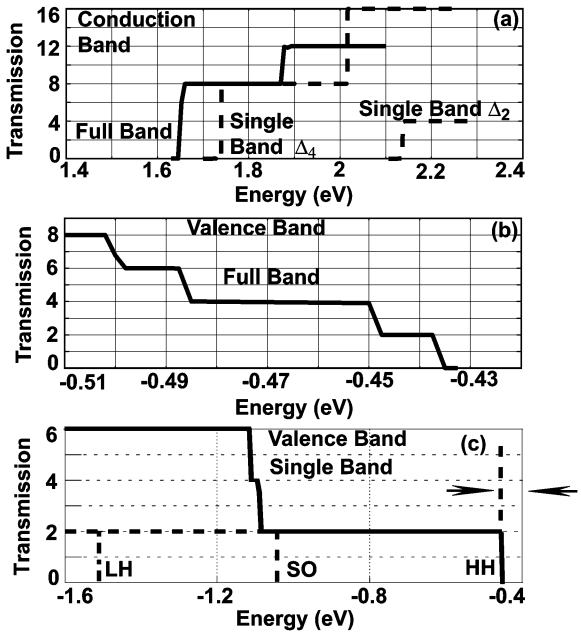

Fig. 8. Transmission versus energy for a 1.54-nm wire. (a) Conduction band calculated in both the fullband and single-band model. (b) Fullband calculation of the valence band transmission. (c) Single-band calculation of valence band transmission.

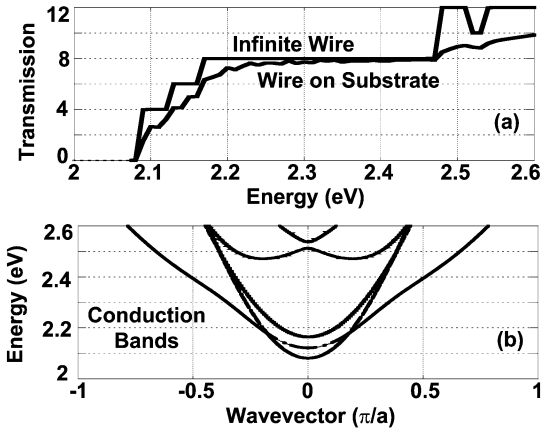

Fig. 9. (a) Comparison of transmission through an ideal wire and wire on substrate calculated in the $sp^3d^5s^*$ model for the 1.15–nm octagonal wire shown on the right in Fig. 1. (b) Conduction band structure of the ideal wire.

falls to 0.31 m_0 for wires thicker than 2.3 nm which is 47% heavier than that of the bulk light-hole. For reference, the bulk valence band [100] masses in this model are $m_{hh} = 0.276\, m_0$, $m_{lh} = 0.214\, m_0$ and $m_{so} = 0.246\, m_0$.

Fig. 8 shows the comparisons of transmission coefficients for the 1.54-nm wire in both the conduction and valence bands, based on the fullband ($sp^3d^5s^*$) model and a single-band model. Fig. 8(a) shows an initial turn on of the conduction band transmission to eight. This corresponds to the eight channels formed by the four valleys and two spins which form the conduction band minimum. The effect of confinement on the conduction band edge is 100 meV larger in the single-band model than in the fullband model. However, the single-band model quickly becomes completely inaccurate at higher energies. The fullband calculation of the transmission coefficient in the valence band is shown in Fig. 8(b). The corresponding single-band calculation is shown in Fig. 8(c). The entire fullband result of Fig. 8(b) lies between the two arrows in Fig. 8(c). The single-band calculation predicts the valence band edge shifted down 18 meV further than the fullband calculation. Nothing else is remotely correct in the single-band calculation for the valence band.

Fig. 9(a) shows a comparison of the calculated transmission coefficients for an ideal wire and a wire on a substrate as shown on the right in Fig. 1. The $E - k$ relation of the ideal wire is shown in Fig. 9(b). The difference between the two transmission coefficients in Fig. 9(a) can be understood if one thinks of the Si wire on bulk Si as a heterostructure. The Si wire is a wider bandgap material than the bulk Si with a conduction band offset of 0.95 eV. Thus, reflection occurs at the bulk-wire interface reducing the transmission coefficient from its ideal values. The dip in the fullband transmission at 2.52 eV occurs when the energy rises above the cusp at Γ in the $E - k$ plot. A transmission channel disappears but immediately turns back on when the energy crosses the minimum right above the cusp. The three steps in the initial turn-on of the transmission are the result of the three-fold splitting of the conduction band minimum. Note that the first step is a factor of four indicating that the lowest energy is two-fold degenerate.

IV. Conclusion

In the conduction band, valley splitting reduces the averaged mobility mass along the axis of the wire, but quantum confinement increases the transverse mass of the conduction band edge. For the wire thickness range that we have considered, the effective mass at the conduction band edge is at least 35% heavier than that of transverse mass of bulk Si. Quantum confinement has the largest effect on the effective masses in the valence band. The effective mass at the valence band edge is at least six times heavier than that of the bulk. The effective mass of the next highest band is even heavier. Small energy splitting also occurs at the conduction band minimum. For wires greater than 1.54-nm thick, the four bulk valleys which compose the conduction band minimum are split into three energies. The center energy is twofold degenerate roughly evenly split between the lowest and highest energy. The single-band model performs reasonably well at calculating the effective band edges for the 1.54-nm wire. However, the accuracy of the single-band calculation quickly becomes nonexistent as one moves away from the band edges. The representation of the valence band with the effective mass model is shown to be meaningless. The wire-substrate interface acts as a heterojunction with a band offset between the bulk and the wire resulting in reflection in the transmission.

We have become aware of earlier work addressing the electrical and optical properties SiNWs motivated by an interest in porous Si[41]–[48]. In particular, [41] and [42] describe second neighbor empirical $sp^3d^2s^*$ electronic bandstructure calculations in qualitative agreement with the results presented here, and [48] uses those results to compute transport properties.

REFERENCES

[1] X. Duan and C. M. Lieber, "General synthesis of compound semiconductor nanowires," *Adv. Mater.*, vol. 12, no. 4, pp. 298–302, 2000.

[2] C. J. Barrelet, Y. Wu, D. C. Bell, and C. M. Lieber, "Synthesis of CdS and ZnS nanowires using single-source molecular precursors," *J. Amer. Chem. Soc.*, vol. 125, no. 38, pp. 11498–9, 2003.

[3] Y. Huang, X. Duan, Y. Cui, and C. M. Lieber, "Gallium nitride nanowire nanodevices," *Nano. Lett.*, vol. 2, no. 2, pp. 101–104, 2002.

[4] Z. Zhong, F. Qian, D. Wang, and C. M. Lieber, "Synthesis of p-type gallium nitride nanowires for electronic and photonic nanodevices," *Nano. Lett.*, vol. 3, no. 3, pp. 343–346, 2003.

[5] Y. Cui, L. J. Lauhon, M. S. Gudiksen, J. Wang, and C. M. Lieber, "Diameter-controlled synthesis of single-crystal silicon nanowires," *Appl. Phys. Lett.*, vol. 78, no. 15, pp. 2214–6, 2001.

[6] A. M. Morales and C. M. Lieber, "A laser ablation method for the synthesis of crystalline semiconductor nanowires," *Science*, vol. 279, pp. 208–211, 1998.

[7] M. S. Gudiksen, J. Wang, and C. M. Lieber, "Size-dependent photoluminescence from single indium phosphide nanowires," *J. Phys. Chem.*, vol. 106, no. 16, pp. 4036–9, 2002.

[8] X. Duan, Y. Huang, Y. Cui, J. Wang, and C. M. Lieber, "Indium phosphide nanowires as building blocks for nanoscale electronic and optoelectronic devices," *Nature*, vol. 409, pp. 66–9, 2001.

[9] Y. Cui, Z. Zhong, D. Wang, W. U. Wang, and C. M. Lieber, "High performance silicon nanowire field effect transistors," *Nano. Lett.*, vol. 3, no. 2, pp. 149–152, 2003.

[10] Y. Cui and C. M. Lieber, "Functional nanoscale electronic devices assembled using silicon nanowire building blocks," *Science*, vol. 291, pp. 851–3, 2001.

[11] J. F. Wang, M. S. Gudiksen, X. F. Duan, Y. Cui, and C. M. Lieber, "Highly polarized photoluminescence and photodetection from single indium phosphide nanowires," *Science*, vol. 293, pp. 1455–1457, 2001.

[12] J. Hahm and C. M. Lieber, "Direct ultrasensitive electrical detection of dna and dna sequence variations using nanowire nanosensors," *Nano. Lett.*, vol. 4, no. 1, pp. 51–54, 2004.

[13] Y. Cui, Q. Wei, H. Park, and C. M. Lieber, "Nanowire nanosensors for highly sensitive and selective detection of biological and chemical species," *Science*, vol. 293, pp. 1289–92, 2001.

[14] X. Duan, Y. Huang, R. Agarwal, and C. M. Lieber, "Single-nanowire electrically driven lasers," *Nature*, vol. 421, pp. 241–5, 2003.

[15] Z. Zhong, D. Wang, Y. Cui, M. W. Bockrath, and C. M. Lieber, "Nanowire crossbar arrays as address decoders for integrated nanosystems," *Science*, vol. 302, pp. 1377–9, 2003.

[16] X. Duan, Y. Huang, and C. M. Lieber, "Nonvolatile memory and programmable logic from molecule-gated nanowires," *Nano. Lett.*, vol. 2, no. 5, pp. 487–490, 2002.

[17] Y. Huang, X. Duan, Q. Wei, and C. M. Lieber, "Directed assembly of one-dimensional nanostructures into functional networks," *Science*, vol. 291, pp. 630–3, 2001.

[18] Y. Huang, X. Duan, Y. Cui, L. J. Lauhon, K.-H. Kim, and C. M. Lieber, "Logic gates and computation from assembled nanowire building blocks," *Science*, vol. 294, pp. 1313–7, 2001.

[19] U. Landman, R. N. Barnett, A. G. Scherbakov, and P. Avouris, "Metal-semiconductor nanocontacts: Silicon nanowires," *Phys. Rev. Lett.*, vol. 85, no. 9, pp. 1958–1961, 2000.

[20] G. J. Evans, H. Mizuta, and H. Ahmed, "Modeling of structural and threshold voltage characteristics of randomly doped silicon nanowires in the coulomb-blockade regime," *Jpn. J. Appl. Phys.*, vol. 40, no. 10, pp. 5837–5840, 2001.

[21] Y.-J. Ko, M. Shin, S. Lee, and K. W. Park, "Effects of atomistic defects on coherent electron transmission in Si nanowires: Full band calculations," *J. Appl. Phys.*, vol. 89, no. 1, pp. 374–379, 2001.

[22] S. G. Volz and G. Chen, "Molecular dynamics simulation of thermal conductivity of silicon nanowires," *Appl. Phys. Lett.*, vol. 75, no. 14, pp. 2056–2058, 1999.

[23] X. Lu and J. H. Chu, "Phonon heat transport in silicon nanowires," *Eur. J. Phys.*, vol. 26, no. 3, pp. 375–378, 2002.

[24] Y. Kanemitsu, H. Sato, S. Nihonyanagi, and Y. Hirai, "Efficient radiative recombination of indirect excitons in silicon nanowires," *Phys. A*, vol. 190, no. 3, pp. 755–758, 2002.

[25] Y. Cui, X. Duan, J. Hu, and C. M. Lieber, "Doping and electrical transport in silicon nanowires," *J. Phys. Chem.*, vol. 104, no. 22, pp. 5213–6, 2000.

[26] P. M. Solomon, J. Jopling, D. J. Frank, C. D'Emic, O. Dokumaci, P. Ronsheim, and W. E. Haensch, "Universal tunneling behavior in technologically relevant p/n junction diodes," *J. Appl. Phys.*, vol. 95, no. 10, pp. 5800–5812, 2004.

[27] M. Lundstrom, "Device physics at the scaling limit: What matters?," in *IEDM Tech. Dig.*, 2003, pp. 33.1.1–4.

[28] J. Guo, S. Datta, M. Lundstrom, M. Brink, P. McEuen, A. Javey, H. Dai, H. Kim, and P. McIntyre, "Assessment of silicon MOS and carbon nanotube FET performance limits using a general theory of ballistic transistors," in *IEDM Tech. Dig.*, Dec. 2002, pp. 711–714.

[29] B. E. Kane, "A silicon-based nuclear spin quantum computer," *Nature*, vol. 393, no. 6681, pp. 133–137, 1998.

[30] B. Koiller, X. Hu, and S. D. Sarma, "Exchange in silicon-based quantum computer architecture," *Phys. Rev. Lett.*, vol. 88, no. 2, pp. 027 903/1–4, 2002.

[31] C. J. Wellard, L. C. L. Hollenberg, F. Parisoli, L. M. Kettle, H.-S. Goan, J. A. L. McIntosh, and D. N. Jamieson, "Electron exchange coupling for single-donor solid-state spin qubits," *Phys. Rev. B, Condens. Matter*, vol. 68, pp. 195 209/1–9, 2003.

[32] C. Rivas, R. Lake, W. R. Frensley, G. Klimeck, P. E. Thompson, K. D. Hobart, S. L. Rommel, and P. R. Berger, "Full-band modeling of the excess current in a delta-doped silicon tunnel diode," *J. Appl. Phys.*, vol. 94, no. 8, pp. 5005–5013, 2003.

[33] R. C. Bowen, W. R. Frensley, G. Klimeck, and R. K. Lake, "Transmission resonances and zeros in multiband models," *Phys. Rev. B, Condens. Matter*, vol. 52, no. 4, pp. 2754–2754, 1995.

[34] T. B. Boykin, "Generalized eigenproblem method for surface and interface states: The complex bands of GaAs and AlAs," *Phys. Rev. B, Condens. Matter*, vol. 54, pp. 8107–8107, 1996.

[35] T. B. Boykin, G. Klimeck, and F. Oyafuso, "Valence band effective-mass expressions in the $sp^3d^5s^*$ empirical tight-binding model applied to a Si and Ge parametrization," *Phys. Rev. B, Condens. Matter*, vol. 69, pp. 115 201/1–10, 2004.

[36] C. Rivas and R. Lake, "Three-dimensional, fullband, quantum modeling of electron and hole transport through Si/SiGe nano-structures," in *Proc. Nanotechnology Conf. Trade Show*, San Francisco, CA, Feb. 2003, pp. 137–140.

[37] J.-M. Jancu, R. Scholz, F. Beltram, and F. Bassani, "Empirical $spds^*$ tight-binding calculation for cubic semiconductors: General method and material parameters," *Phys. Rev. B, Condens. Matter*, vol. 57, no. 11, pp. 6493–6507, 1998.

[38] S. Lee, F. Oyafuso, P. von Allmen, and G. Klimeck, "Boundary conditions for the electronic structure of finite-extent embedded semiconductor nanostructures," *Phys. Rev. B, Condens. Matter*, vol. 69, no. 4, pp. 045 316–045 316, 2004.

[39] C. Rivas and R. Lake, "Non-equilibrium green function implementation of boundary conditions for fullband simulations of substrate-nanowire structures," *Phys. B*, vol. 239, no. 1, pp. 94–102, 2003.

[40] T. B. Boykin, G. Klimeck, M. A. Eriksson, M. Friesen, S. N. Coppersmith, P. V. Allmen, F. Oyafuso, and S. Lee, "Valley splitting in strained silicon quantum wells," *Appl. Phys. Lett.*, vol. 84, no. 1, pp. 115–117, 2004.

[41] G. D. Sanders *et al.*, "Optical properties of free-standing silicon quantum wires," *Appl. Phys. Lett.*, vol. 60, no. 20, pp. 2525–2527, 1992.

[42] G. D. Sanders, "Theory of optical properties of quantum wires in porous silicon," *Phys. Rev. B, Condens. Matter*, vol. 45, no. 16, pp. –9213, 1992.

[43] M. S. Hybertson *et al.*, "First-principles analysis of electronic states in silicon nanoscale quantum wires," *Phys. Rev. B, Condens. Matter*, vol. 48, no. 7, pp. 4608–4611, 1993.

[44] A. J. Read *et al.*, "First-principles calculations of the electronic properties of Si quantum wires," *Phys. Rev. Lett.*, vol. 69, no. 8, pp. 1232–1235, 1992.

[45] T. Ohno, "Intrinsic origin of visible light emission from silicon quantum wires: Electronic structure and geometrically restricted exciton," *Phys. Rev. Lett.*, vol. 69, no. 16, pp. 2400–2403, 1992.

[46] F. Buda *et al.*, "Optical properties of porous silicon: A first-principles study," *Phys. Rev. Lett.*, vol. 69, no. 8, pp. 1272–1275, 1992.

[47] C. Delerue *et al.*, "Theoretical aspects of the luminescence of porous silicon," *Phys. Rev. B, Condens. Matter*, vol. 48, no. 15, pp. 11024–11036, 1993.

[48] G. D. Sanders *et al.*, "Theory of transport in sislicon quantum wires," *Phys. Rev. B, Condens. Matter*, vol. 48, no. 15, pp. 11067–11076, .

Yun Zheng received the B.S. (with highest honors) and M.S. degrees in electrical engineering from Xi'an University of Technology (XUT), Xi'an, China, in 1994 and 1998, respectively. She received an M.S. degree in electrical engineering from the University of California, Riverside (UCR) in 2003.

From 1994 to 1999, she was a Lecturer with the Information Science Department, XUT.

Cristian Rivas received the degree from the University of Texas at Dallas, Richardson, where he performed research in the area of computational microelectronics.

He is currently investigating high-frequency effects in SiC material and devices in collaboration with Mississippi State University, Mississippi State.

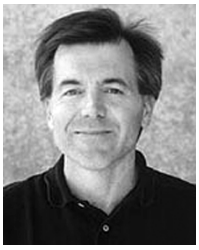

Roger Lake (SM'01) received the Ph.D. degree in electrical engineering from Purdue University, West Lafayette, IN, in 1992.

He joined the Nanoelectronics Branch of Central Research Laboratories, Texas Instruments, Dallas, TX, in 1993 to develop the theory for the Nanotechnology Engineering Program, which became known as NEMO. In 1997, the Nanoelectronics Branch was acquired by Raytheon, where he worked on different materials and devices, including Si–SiGe tunnel diodes, InGaAs–InAlAs HEMTs, InAs–AlSb and InGaAs–InAs–AlAs RTDs for ADC, TSRAM, and terahertz applications. In 2000, he joined the Electrical Engineering Department, University of California, Riverside and started the laboratory for terahertz and terascale electronics (LATTE) for investigating future electronic materials and devices.

Khairul Alam (M'04) received the B.S. and M.S. degrees in electrical engineering from Bangladesh University of Engineering and Technology, Bangladesh, India, in 1999 and 2002, respectively. He is currently pursuing the Ph.D. degree in electrical engineering at the University of California, Riverside.

His research focuses on the electronic transport in nanoscale devices, especially carbon nanotube transistors and silicon nanowires.

Timothy B. Boykin (M'85) received the B.S. degree (*summa cum laude*) from Rice University, Houston, TX, in 1987, the M.S. degree in 1988, and the Ph.D. degree in 1992 from Stanford University, Stanford, CA, all in electrical engineering.

He is an Associate Professor in the Department of Electrical and Computer Engineering (ECE), University of Alabama, Huntsville (UAH). He joined the ECE Department of UAH in September, 1992, was promoted to Associate Professor in August, 1997, and awarded tenure in August, 1998. His research centers on detailed semiconductor heterostructure and device modeling. Highlights of his research include the first numerically stable localized-orbital basis heterostructure model, the impact of nonzero in-plane wavevector on tunneling, incompleteness in tight-binding models, improved methods for calculating boundary conditions in tight-binding models, optimizations and capabilities of tight-binding models, consequences of incompleteness for the quantum–mechanical continuity equation, the representation of electromagnetic effects in tight-binding models, and valley splitting in silicon quantum wells. He has authored or coauthored over forty refereed journal articles and his first-authored papers alone have been cited by other (non-coauthor) researchers over 240 times.

Dr. Boykin is a member of Phi Beta Kappa, Tau Beta Pi, Eta Kappa Nu, the American Physical Society, and Sigma Xi. In 2001, he won the UAH Foundation Award for Research and Creative Achievement in Applied Science/Technology.

Gerhard Klimeck (M'95) received the degree in electrical engineering from Ruhr-University Bochum, Germany, in 1990, and the Ph.D. degree from Purdue University, West Lafayette, IN, in 1994.

He is the Technical Director of the Network for Computational Nanotechnology at Purdue University and a Professor of Electrical and Computer Engineering since 2003. He leads the development and deployment of web-based simulation tools that are hosted on http://nanohub.org, a community website utilized by over 5000 users annually. He was the Technical Group Supervisor for the Applied Cluster Computing Technologies Group and continues to hold his appointment as a Principal Member at the Jet Propulsion Laboratory, California Institute of Technology, on a faculty part-time basis. His research interest is in the modeling of nanoelectronic devices, parallel cluster computing, genetic algorithms, and parallel image processing. He has been the lead on the development of NEMO 3-D, a tool that enables the simulation of multimillion atom quantum dot systems, and NEMO 1-D, the first nanoelectronic CAD tool. Previously, he was a Member of Technical Staff at the Central Research Lab, Texas Instruments, Dallas, TX. His work is documented in over 120 peer-reviewed publications and over 190 conference presentations.

Dr. Klimeck is a member of APS, HKN, and TBP.